Received: 29 September 2023

# RESEARCH ARTICLE







Check for updates

# Chemical bonding in Uranium-based materials: A local vibrational mode case study of Cs<sub>2</sub>UO<sub>2</sub>Cl<sub>4</sub> and UCl<sub>4</sub> crystals

Filippo Bodo 1,2 | Alessandro Erba 2 | Elfi Kraka 1 | Renaldo T. Moura Jr. 1,3 |

### Correspondence

Renaldo T. Moura Jr., Computational and Theoretical Chemistry Group (CATCO), Department of Chemistry, Southern Methodist University, Dallas, TX 75275-0314, USA. Email: renaldo.mourajr@cca.ufpb.br

### Abstract

The Local Vibrational Mode Analysis, initially applied to diverse molecular systems, was extended to periodic systems in 2019. This work introduces an enhanced version of the LModeA software, specifically designed for the comprehensive analysis of two and three-dimensional periodic structures. Notably, a novel interface with the CRYSTAL package was established, enabling a seamless transition from molecules to periodic systems using a unified methodology. Two distinct sets of uranium-based systems were investigated: (i) the evolution of the Uranyl ion  $(UO_2^{2+})$  traced from its molecular configurations to the solid state, exemplified by Cs<sub>2</sub>UO<sub>2</sub>Cl<sub>4</sub> and (ii) Uranium tetrachloride (UCl<sub>4</sub>) in both its molecular and crystalline forms. The primary focus was on exploring the impact of crystal packing on key properties, including IR and Raman spectra, structural parameters, and an in-depth assessment of bond strength utilizing local mode perspectives. This work not only demonstrates the adaptability and versatility of LModeA for periodic systems but also highlights its potential for gaining insights into complex materials and aiding in the design of new materials through fine-tuning.

### KEYWORDS

bond strength, chemical bonding, crystalline systems, local vibrational mode analysis, uraniumbased materials

#### INTRODUCTION 1

The concept of the chemical bond, which describes the interaction between atoms in molecules, holds immense significance in chemistry. 1-3 Over the years, a wide range of methods characterizing and assessing the nature and strength of chemical bonds have gained popularity. Two prominent methods aiming at establishing a connection between the concept of the chemical bond and the quantum nature of electrons are the NBO (Natural Bond Orbital) analysis<sup>4–8</sup> and Bader's Quantum Theory of Atoms In Molecules (QTAIM).9-14 The Bond Dissociation Energy (BDE)<sup>15-17</sup> is widely used in chemistry to assess the strength of a chemical bond. Although the BDE offers valuable intuitive insights into chemical bonding, one should consider that it is a reaction parameter; that is, it encompasses various factors associated with the bond dissociation process, including electron

density reorganization and geometry relaxation. Consequently, it is not suitable as a quantitative bond strength descriptor. 18,19 This limitation becomes particularly evident in complex systems such as solidstate materials, where bond breaking can induce significant changes in the overall geometry. Therefore, employing a bond strength descriptor that effectively reflects the electronic properties responsible for the bonding situation in such systems is crucial.

The local vibrational mode (LVM) theory, originally introduced by Konkoli and Cremer<sup>20</sup> and extensively developed in our group<sup>21-23</sup> is a powerful tool for extracting electronic structure information from vibrational spectroscopy data. In particular, the local mode bond stretching force constant (ka) has turned out to be a powerful measure of the intrinsic strength of a chemical bond or weak chemical interaction.<sup>24,25</sup> It can be derived from local vibrational modes<sup>20,26-28</sup> and for a given bond, it represents the curvature of the Potential

<sup>&</sup>lt;sup>1</sup>Computational and Theoretical Chemistry Group (CATCO), Department of Chemistry, Southern Methodist University, Dallas Texas USA

<sup>&</sup>lt;sup>2</sup>Dipartimento di Chimica, Università di Torino,

<sup>&</sup>lt;sup>3</sup>Department of Chemistry and Physics, Center of Agrarian Sciences, Federal University of Paraiba, Areia, Brazil

Energy Surface (PES) along the direction of infinitesimal stretching of that bond, followed by the relaxation of the remaining parts of the molecule.<sup>29</sup>

Since its inception, LVM theory has found successful applications in characterizing a wide range of systems, providing valuable insights into covalent bonding as well as non-covalent interactions involving hydrogen, chalcogen, pnicogen, and unusual chemical bonding phenomena. LVM analysis has also led to a new way of analyzing vibrational spectra, enabling novel investigations such as the examination of pK<sub>a</sub> probes, gaining insights into vibrational Stark effect probes, analyzing characteristic vibrational coupling in nucleobases and Watson-Crick base pairs of DNA, assessing bond strength in biological systems through QM/MM, as evaluating underlying properties of lanthanide compounds, are studying protein-ligand hydrogen bond strength patterns, so just to name a few.

In the realm of periodic systems, various tools have been developed to analyze chemical bonds. Among these methods, QTAIM has gained widespread use for investigating bonding features in solid-state systems.<sup>36–39</sup> QTAIM involves decomposing the molecular electron density into atomic basins, allowing for the determination of paths connecting bonded atoms. By examining the bond critical points and their associated paths, numerous bond-related descriptors can be derived in both molecular and crystalline environments.<sup>9,11</sup> QTAIM provides valuable insights into the nature of chemical bonds in periodic systems, facilitating a comprehensive understanding of their structural and electronic characteristics.

In 1997, Marzari and colleagues introduced the maximally localized Wannier functions (MLWF) method as an alternative approach for analyzing chemical bonding in periodic systems. 40-43 MLWF are utilized to replace the traditional Bloch wavefunctions, to localize the band structure into so-called MLWF-orbitals. The crystal orbital Hamiltonian population (COHP)<sup>44</sup> and crystal orbital overlap population<sup>45</sup> (COOP) also provide a viable option to characterize the chemical bond in periodic systems.<sup>46</sup> These two techniques are almost identical in their formulation and they work similarly to conventional density of states (DOS) calculation, but instead of considering the contributions from all orbitals in a molecular or periodic system, they enable the study of specific interaction pairs between two sets of orbitals.<sup>47</sup> COOP and COHP schemes allows for quantifying the orbital overlap and the strength of interatomic bonds.<sup>48</sup> These methods offer valuable insights into the bonding characteristics in periodic systems, providing a detailed analysis of specific orbital interactions.

Since the 1950s, the pursuit of calculating force constants associated with adjacent atoms in solid-state systems has been a subject of great interest. Pioneering work by Waser and Pauling laid the foundation for understanding the relationships between solid-state compressibility, interatomic distances, and force constants of adjacent atoms. <sup>49</sup> Over the years, this field has witnessed significant advancements, fueling our comprehension of the intricate interactions and behaviors of atoms within solid-state materials. Sophisticated computational methods and cutting-edge experimental techniques have been developed to unravel the complexities of these force constants and their impact on the physical properties of materials. <sup>50</sup> These

approaches encompass a diverse range of methods, including the study of highly localized phonon modes, parameterizations related to solid-state underlying properties, <sup>51-53</sup> determination of mean force constants from phonon density of states, utilizing subblock of the Hessian matrix, <sup>54,55</sup> and calculations of rigid force constants based on bonding atoms displacements. <sup>56,57</sup> For instance, a deeper understanding of solid-state force constants enables the design and optimization of advanced materials with tailored mechanical, thermal, and electrical properties.

Despite these remarkable advancements, the accurate determination of force constants for solid-state systems remains a challenging endeavor, particularly when dealing with complex and multi-component systems. In 2019, an important advance occurred when the local vibrational mode theory was successfully extended to periodic systems. This extension paved the way for a proper characterization of the intrinsic bond strength in solid-state materials. To facilitate the exploration of LVM properties for solid-state systems, a PyMOL plugin was introduced. However, it comes with certain limitations, including usage restricted to hand-made fragment selections and a focus on bond and angle local mode parameters.

In this study, we introduce an enhanced version of the Local Vibrational Mode software package LModeA,<sup>59</sup> tailored specifically for analyzing two and three-dimensional (2D/3D) periodic systems. The upgraded capabilities of LModeA enable a more comprehensive understanding of vibrational modes within these materials. Moreover, a novel interface between LModeA and the CRYSTAL package<sup>60</sup> was developed, facilitating an efficient and user-friendly LVM analysis of periodic systems calculated with ab initio model chemistry. This interface represents a significant advancement in solid-state vibrational computation, opening up exciting possibilities for investigating different classes of materials. To showcase its effectiveness, we investigated two different sets of uranium systems: the evolution of the uranyl ion ( $UO_2^{2+}$ ) from its molecular forms ( $UO_2^{2+}$  and  $UO_2Cl_4^{2-}$ ) to the periodic one (Cs<sub>2</sub>UO<sub>2</sub>Cl<sub>4</sub>, C2/m, no. 15), and uranium tetrachloride (UCl<sub>4</sub>) both in its molecular and crystalline form (I4<sub>1</sub>/amd, no. 141), exploring, in particular, the effects on chemical bonding related to crystal packing effects present in the solid-state. The choice of such system to showcase the newly implemented interface is due to the experience acquired from previous work of some of the authors.<sup>37</sup> Furthermore, the fact that actinide bonding is yet to be full understood,61-63 the growing interest in nuclear power plants, and nuclear waste management<sup>64,65</sup> make the choice of this material even more compelling.

# 2 | METHODOLOGY

# 2.1 | Local vibrational mode theory

The LVM theory is designed to extract local vibrational mode information from the normal vibrational modes. These modes are typically delocalized in molecular systems and solids due to their inherent nature, as previously highlighted by Wilson in 1941 and further

elaborated in the seminal work on vibrational spectroscopy by Wilson, Decius, and Cross in 1955.<sup>67</sup> In their original work, Konkoli and Cremer<sup>20,26–28</sup> derived the local vibrational mode  $a_n$  of molecular fragment  $\phi_n$  being described by an internal parameter  $q_n$  (e.g., bond length, bond angle, torsion, etc.) from the infinitesimal change of  $q_n$  followed by the relaxation of the remaining part of the molecule. For a molecular system being composed of N atoms, for each set of  $N_{vib}$  non-redundant local mode parameters  $q_n$ , with  $n=1,2,...,N_{vib}$  ( $N_{vib}=3N-N_{tr}$  and  $N_{tr}=5$  or 6 for linear and non-linear molecules), there exist a one-to-one relationship between local and normal vibrational modes via an Adiabatic Connection Scheme (ACS), allowing a smooth transition from local to normal modes,<sup>68</sup> and in this way providing a solid physical foundation of LVM theory.

In 2019, LVM theory was extended to one, two, and three-dimensional periodic systems (1D, 2D, and 3D, respectively)<sup>69</sup> with N atoms in the primitive cell and  $N_{vib}=3N-4$  for 1D and 3N-3 for 2D and 3D systems.<sup>70</sup> The authors<sup>69</sup> defined  $a_n$ , in analogy to the molecular system, as the infinitesimal change of an internal coordinate  $q_n$  within the primitive cell, followed by the relaxation of the rest of the cell. Important to note is that the LVM extension was made at the  $\Gamma$  point ( $\mathbf{k}$ = (0, 0, 0)) where phonon vibrational modes can exhibit IR and/or Raman activity,<sup>71</sup> allowing their experimental measurement.

The internal coordinate  $q_n$  defining the local modes is derived from the local mode parameters obtained in the LVM analysis. Specifically, if one provides a local mode parameter for a bond, angle, or dihedral, then  $q_n$  is established as the corresponding local mode, representing either bond stretching, angular, or dihedral deformation, respectively. It is crucial to emphasize that the extension presented in this work does not rely on infinitesimal changes of a given  $q_n$ . Instead, it takes into account that all atoms not involved in the local mode parameter are treated as massless. This approach aligns with the propositions put forth by Cremer<sup>20,26–28</sup> and Kraka. <sup>21,69</sup> The subsequent sections will elucidate the procedure for determining  $a_n$  based on this assumption, drawing an analogy to the molecular case.

Starting from the force constant matrix  $\mathbf{F}$ , details regarding the  $N_{\text{vib}}$  vibrational frequencies and the specific movements of atoms during a given vibration can be extracted using the Wilson GF machinery. This involves solving the vibrational secular equation, as outlined by Wilson,<sup>67</sup> Woodward,<sup>72</sup> Califano,<sup>73</sup> and in various vibrational spectroscopy review works.<sup>74</sup> Here, GF refers to Wilson's inverse kinetic energy matrix  $\mathbf{G}$  (to be defined subsequently) and the force constant matrix  $\mathbf{F}$ . Expressed in Cartesian coordinates  $\mathbf{x}$ , with  $x_i = 1, 2, ..., 3N$  this equation takes the following form,

$$\mathbf{F}^{\mathbf{x}}\tilde{\mathbf{L}} = \mathbf{M}\tilde{\mathbf{L}}\mathbf{\Lambda}$$
 (1)

where matrix  $\hat{\bf L}$  collects the  $N_{vib}$  vibrational eigenvectors  ${\bf I}_{\mu}$  in its columns.  ${\bf \Lambda}$  is a diagonal matrix with the eigenvalues  $\lambda_{\mu}$ , connected to the harmonic vibrational frequencies  $\omega_{\mu}$  according to  $\lambda_{\mu}=4\pi^2c^2\omega_{\mu}^2$ , c is the speed of light.  ${\bf M}$  is the diagonal mass matrix of the molecule in question which contains each atomic mass three times to account for the motion in the x, y and z direction, respectively, that is,  $M_{i,j}=\{m_1,m_1,m_2,m_2,m_2,m_2,...\}$ . The tilde above a vector or matrix

symbol indicates mass-weighting. Matrix  $\tilde{\textbf{L}}$  has the following properties

$$\tilde{\mathbf{L}}^{\dagger}\mathbf{M}\tilde{\mathbf{L}} = \mathbf{I}$$
 (2)

$$\tilde{\mathbf{L}}^{\dagger} \mathbf{F}^{\mathbf{x}} \tilde{\mathbf{L}} = \mathbf{\Lambda} \tag{3}$$

that is, matrix  $\tilde{\mathbf{L}}$  and eigenvalue matrix  $\boldsymbol{\Lambda}$  are obtained by diagonalization of the force constant matrix. Usually, the normal mode vectors  $\tilde{\mathbf{I}}_{\mu}$  are re-normalized according to

$$I_{\mu} = \frac{1}{\sqrt{\tilde{l}_{\mu}^{\dagger}}\tilde{l}_{\mu}}\tilde{l}_{\mu} = \sqrt{m_{\mu}^{R}}\tilde{l}_{\mu} \tag{4}$$

where  $m_{\mu}^{R} = \left(\tilde{l}_{\mu}^{\dagger}\tilde{l}_{\mu}\right)^{-1}$  is the reduced mass of mode  $\mu$ . Equation (4) expressed in matrix form leads to  $\mathbf{L} = \tilde{\mathbf{L}} \left(\mathbf{M}^{R}\right)^{1/2}$ .

Matrix L also satisfies Equation (1) which leads to

$$\mathbf{L}^{\dagger}\mathbf{F}^{\mathbf{x}}\mathbf{L} = \mathbf{K} \tag{5}$$

$$\mathbf{L}^{\dagger}\mathbf{M}\mathbf{L} = \mathbf{M}^{R} \tag{6}$$

Equations (5) and (6) define the diagonal normal force constant matrix  $\mathbf{K}$  in normal coordinates  $\mathbf{Q}$  and the reduced mass matrix  $\mathbf{M}^R$  (with elements  $m_n^R$ ), respectively.

The vibrational secular equation can also be expressed in internal coordinates  $q_n^{67}$ 

$$\mathbf{F}^q \tilde{\mathbf{D}} = \mathbf{G}^{-1} \tilde{\mathbf{D}} \Lambda \tag{7}$$

 $\tilde{\mathbf{D}}$  contains the normal mode vectors  $\tilde{\mathbf{d}}_{\mu}$  ( $\mu=1,...,N_{vib}$ ). The real symmetric matrix  $\mathbf{G}$  is the Wilson  $\mathbf{G}$  matrix,<sup>67</sup> the so-called inverse kinetic energy matrix, with off-diagonal elements of the form  $G_{ij}=G_{ji}$  describing the kinetic coupling between modes i and j. Renormalization of  $\tilde{\mathbf{D}}$  according to  $\mathbf{D}=\tilde{\mathbf{D}}$  ( $\mathbf{M}^R$ )<sup>1/2</sup> leads to

$$\mathbf{F}^{q}\mathbf{D} = \mathbf{G}^{-1}\mathbf{D}\mathbf{\Lambda} \tag{8}$$

$$\mathbf{D}^{\dagger}\mathbf{F}^{q}\mathbf{D} = \mathbf{K} \tag{9}$$

$$\mathbf{D}^{\dagger}\mathbf{G}^{-1}\mathbf{D} = \mathbf{M}^{R} \tag{10}$$

Cartesian and internal coordinate systems are connected by the following equations:

$$\mathbf{F}^{\mathbf{q}} = \mathbf{C}^{\dagger} \mathbf{F}^{\mathbf{x}} \mathbf{C} \tag{11}$$

$$\mathbf{G} = \mathbf{B} \mathbf{M}^{-1} \mathbf{B}^{\dagger} \tag{12}$$

$$D = BL \tag{13}$$

The rectangular Wilson **B** matrix provides the relationship between internal and Cartesian coordinates via the first derivatives of

the internal coordinates  $q_n$  ( $n = 1, 2, 3..., N_{vib}$ ) with regard to the Cartesian coordinates  $x_i$  (i = 1, 2, 3..., 3N),

$$\mathbf{B}_{n} = \frac{\delta q_{n}(\mathbf{x})}{\delta x_{i}} \tag{14}$$

Important to note is that this can be extended to other coordinates, such as curvilinear coordinates, used to describe inversion and bond pseudo-rotation in Jahn-Teller systems,  $^{75-77}$  or Cremer-Pople ring puckering coordinates,  $^{78}$  or the  $\pi$ -interaction between transition metal and ring ligands in sandwich complexes  $^{79-81}$  and so forth, as long as the  $\mathbf{B}_n$  vector can be derived according to Equation (14) for the coordinate n under consideration.

After a standard normal mode analysis<sup>82,83</sup> which is offered by most modern quantum chemistry package for molecular and solid state calculations, providing as an output the diagonal force constant matrix  $\mathbf{K}$  and the normal mode vectors  $\mathbf{d}_{\mu}$ , the subsequent determination of local vibrational modes  $\mathbf{a}_n$  is straightforward:<sup>21,22</sup>

$$\mathbf{a}_{n} = \frac{\mathbf{K}^{-1} \mathbf{d}_{n}^{\dagger}}{\mathbf{d}_{n} \mathbf{K}^{-1} \mathbf{d}_{n}^{\dagger}} \tag{15}$$

where Equation (15) clearly shows that the local vibrational mode  $\mathbf{a}_n$  is fully determined by the diagonal force constant matrix  $\mathbf{K}$  in normal coordinates  $\mathbf{Q}$  and the n-th row vector  $\mathbf{d}_n$  of the normal mode matrix  $\mathbf{D}$  in internal coordinates  $\mathbf{q}_n$ .

To each local vibrational mode  $\mathbf{a}_n$ , the corresponding local mode frequency  $\omega_n^a$  and local force constant  $k_n^a$  can be defined by:

$$\omega_n^a = \frac{1}{2\pi c} \sqrt{\frac{k_n^a}{m_n^a}} \tag{16}$$

and the corresponding local force constant  $k_n^a$  by:

$$k_n^a = (\mathbf{d}_n \mathbf{K}^{-1} \mathbf{d}_n^{\dagger})^{-1}, \ \mathbf{d}_n = \mathbf{B}_n \mathbf{L}$$
 (17)

where  $m_n^a$  in Equation (16) corresponds to the local mode mass. <sup>21,22</sup>

Local mode force constants exhibit sensitivity to variations in electronic structure, for instance, induced by changes in substituents.<sup>21</sup> Due to their independence from atomic masses, these force constants effectively capture pure electronic effects. Specifically, the local stretching force constant  $k_n^a$  (pertaining to a bond AB in an R-A-B-R' molecular system) serves as an indicator of the intrinsic strength of the bond/interaction between atoms A and B, described by an internal coordinate  $q_n$ ,  $k_n^a$  is strictly linked to the second derivative of the molecular energy concerning  $q_n$ , representing the curvature of the Born-Oppenheimer PES along the direction defined by  $q_n$ . Zou and Cremer<sup>84</sup> demonstrated that by approximating the PES in the  $q_n$ direction with a Morse potential and maintaining the electron density frozen during the dissociation process, the intrinsic bond strength becomes directly proportional to  $k_n^a$ . Consequently, justifying the consideration of  $k_n^a$  as a unique and universal measure of the intrinsic strength of a chemical bond based on vibrational spectroscopy.

Generally speaking, in solid state the calculation are performed on the primitive cell (Figure 1A,B) that can be extracted from the conventional one through a transformation matrix, <sup>85</sup> often included in the *ab-initio* code of choice. Thus, all of the aforementioned post-processing is performed on the primitive cell defined by the user in the frequency calculation input. A fundamental requirement of the LVM theory is that the internal coordinates of interest (i.e., bonds, bond angles and dihedral angles) are within the cell boundaries. This condition, though, is not necessarily fulfilled by all primitive cells. Thus, we can choose between two possible approaches: (i) a shift of the cell origin (Figure 1D), or (ii) a supercell approach (Figure 1C). In the first case, the primitive cell maintains its dimensions, while its origin is shifted by a fraction of the cell parameters to include the internal coordinate(s) of interest, as shown in Figure 1D. In the supercell approach, instead, a larger cell is defined through an expansion matrix

$$\mathbf{P} = \begin{pmatrix} P_{11} & P_{12} & P_{13} \\ P_{21} & P_{22} & P_{23} \\ P_{31} & P_{32} & P_{33} \end{pmatrix} \tag{18}$$

acting on the primitive lattice vectors ( $\mathbf{a}$ ,  $\mathbf{b}$  and  $\mathbf{c}$ ) to generate the supercell lattice vectors ( $\mathbf{a}'$ ,  $\mathbf{b}'$  and  $\mathbf{c}'$ ) as:

$$(\mathbf{a'} \ \mathbf{b'} \ \mathbf{c'}) = (\mathbf{a} \ \mathbf{b} \ \mathbf{c}) \begin{pmatrix} P_{11} \ P_{12} \ P_{13}, \\ P_{21} \ P_{22} \ P_{23}, \\ P_{31} \ P_{32} \ P_{33}, \end{pmatrix} = \begin{pmatrix} P_{11}\mathbf{a} + P_{21}\mathbf{b} + P_{31}\mathbf{c}, \\ P_{12}\mathbf{a} + P_{22}\mathbf{b} + P_{32}\mathbf{c}, \\ P_{13}\mathbf{a} + P_{23}\mathbf{b} + P_{33}\mathbf{c} \end{pmatrix}$$

$$(19)$$

so that

$$\mathbf{a}' = P_{11}\mathbf{a} + P_{21}\mathbf{b} + P_{31}\mathbf{c} \tag{20}$$

$$\mathbf{b}' = P_{12}\mathbf{a} + P_{22}\mathbf{b} + P_{32}\mathbf{c} \tag{21}$$

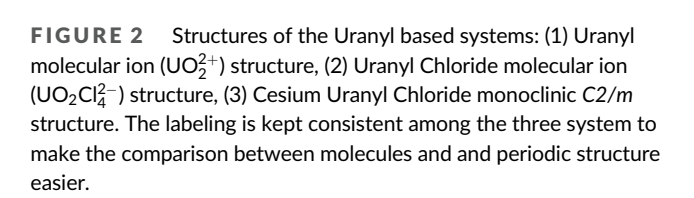
$$\mathbf{c}' = P_{13}\mathbf{a} + P_{23}\mathbf{b} + P_{33}\mathbf{c} \tag{22}$$

Therefore, the lattice vectors of the supercell are effectively expressed as linear combinations of the primitive ones. Furthermore, in this case the calculation is performed on the  $\Gamma$  point of the supercell which folds in itself the information related to the Brillouin zone beyond the primitive  $\Gamma$  point.

Among the two approaches, it is advisable to use the first one whenever possible due to its lower computational cost and the preservation of all the symmetry operators.

# 2.2 | Computational details

Both molecular and solid-state calculations from Crystal package were taken into consideration. In the first case study, three test systems are considered. Test system 1 (Figure 2) revolved around the molecular uranyl ion ( $UO_2^{2+}$ ), and in test system 2, chlorine atoms are introduced to examine the effects on bond stretching and angular deformation in



[UO<sub>2</sub>]<sup>2+</sup>

Cs 🔘 U

O CI O O

(A) (B) Cell Origin Shirt (C)

FIGURE 1 Evolution from the conventional cell to the possible cell choice for LModeA calculation: (A) Conventional/Primitive cell of a Urea crystal where in its tetragonal lattice. (B) Primitive cell considered for the calculation where all of the contribution have been collapsed into two Urea molecules. (C) A "2 2 2" supercell of Urea obtained translating the primitive cell along the three lattice vectors with the red lines outlining the supercell. (D) Representation of a primitive cell that underwent a 0.25a and 0.25c shift of the origin.

the uranyl chloride molecular ion  $(UO_2Cl_4^2)$ . Building upon this, test systems 1 and 2 were further developed to explore the crystal packing effects in the Cs<sub>2</sub>UO<sub>2</sub>Cl<sub>4</sub> solid-state environment, leading us to investigate test system 3 (Figure 2). In the second case study, we focused on the impact of crystal packing on the U-Cl chemical bond in both molecular calculations and a solid-state environment, specifically analyzing the UCl<sub>4</sub> unit.

All the calculations discussed in this work were conducted on the fully relaxed structures of the test systems. The only constraints applied were the C2/m and I4<sub>1</sub>/amd symmetry imposed by the monoclinic and tetragonal space groups of Cs<sub>2</sub>UO<sub>2</sub>Cl<sub>4</sub> and UCl<sub>4</sub>, respectively.

All geometry optimization and frequency calculations were conducted using a developmental version of the Crystal 23 package. 60 The global hybrid B3LYP exchange-correlation functional<sup>86</sup> and a

 $6 \times 6 \times 6$  Monkhorst-Pack grid were employed for these calculations. The Uranyl ion  $UO_2^{2+}$ ,  $UO_2Cl_4^{2-}$ , and  $Cs_2UO_2Cl_4$  systems were described utilizing the ECP60MDF small-core pseudopotential<sup>87,88</sup> for U, which accounted for scalar relativistic effects. 89,90 The Uranium valence electrons were described by a fully uncontracted (10s9p7d5f1g)/[10s9p7d5f1g] basis.<sup>37</sup>

Chlorine and Oxygen were described using the molecular def2-TZVP basis set, with (14s9p3d1f)/[5s5p2d1f] and (11s6p2d1f)/ [5s3p2d1f] types, respectively.<sup>5</sup> Cesium atoms were described using the Hay-Wadt small-core pseudopotential<sup>91</sup> in combination with a (4s4p1d)/[2sp1d] valence basis set. The same basis set combination used for Uranium and Chlorine was also applied to the UCl₄ systems. However, in this case, the molecular structure was extracted from the crystalline system using the keyword MOLECULE, 92 and then fully relaxed to achieve the equilibrium structure.

To overcome the absence of some of the internal coordinates of interest in the primitive cell of the two solid state systems, we have used a supercell approach using the SUPERCEL keyword<sup>92</sup> in CRYSTAL. In the Cs<sub>2</sub>UO<sub>2</sub>Cl<sub>4</sub> case, the selected supercell was

$$\begin{pmatrix} 2 & 1 & 1 \\ 1 & 2 & 1 \\ 1 & 1 & 2 \end{pmatrix} \tag{23}$$

while in the Uranium tetra-Chloride, the supercell used was

$$\begin{pmatrix} 2 & 0 & 0 \\ 0 & 1 & 0 \\ 0 & 0 & 1 \end{pmatrix} \tag{24}$$

Additionally, the second derivatives required for the computation of the Hessian matrix were evaluated numerically with a central difference formula to improve the accuracy, changing the default setting of the NUMDERIV keyword. 92 To further improve the accuracy of the calculation we used tighter tolerances on Coulomb and Exchange integrals setting the TOLINTEG to 8 8 8 8 16.92 Moreover, the

.096987x, 0, Downloaded from https://onlinelibrary.wiley.com/doi/10.1002/jcc.27311 by Southern Methodist University, Wiley Online Library on [13/03/2024]. See the Terms

ns) on Wiley Online Library for rules of use; OA articles are governed by the applicable Creative Commons

convergence was reached when the difference in energy between two successive cycles did not exceed  $1 \times 10^{-9}$  Ha and a pruned grid consisting of 99 radial point and 1454 angular points was used for integration through the XXLGRID keyword. 92

#### 3 RESULTS AND DISCUSSION

We will now proceed with the discussion of the results obtained for the two case studies considered. The discussion will be divided into two sections one for each set of system where we will analyze the packing effects of two periodic system using IR and Raman spectroscopy showcasing how these effects are also reflected in the calculated adiabatic force constants.

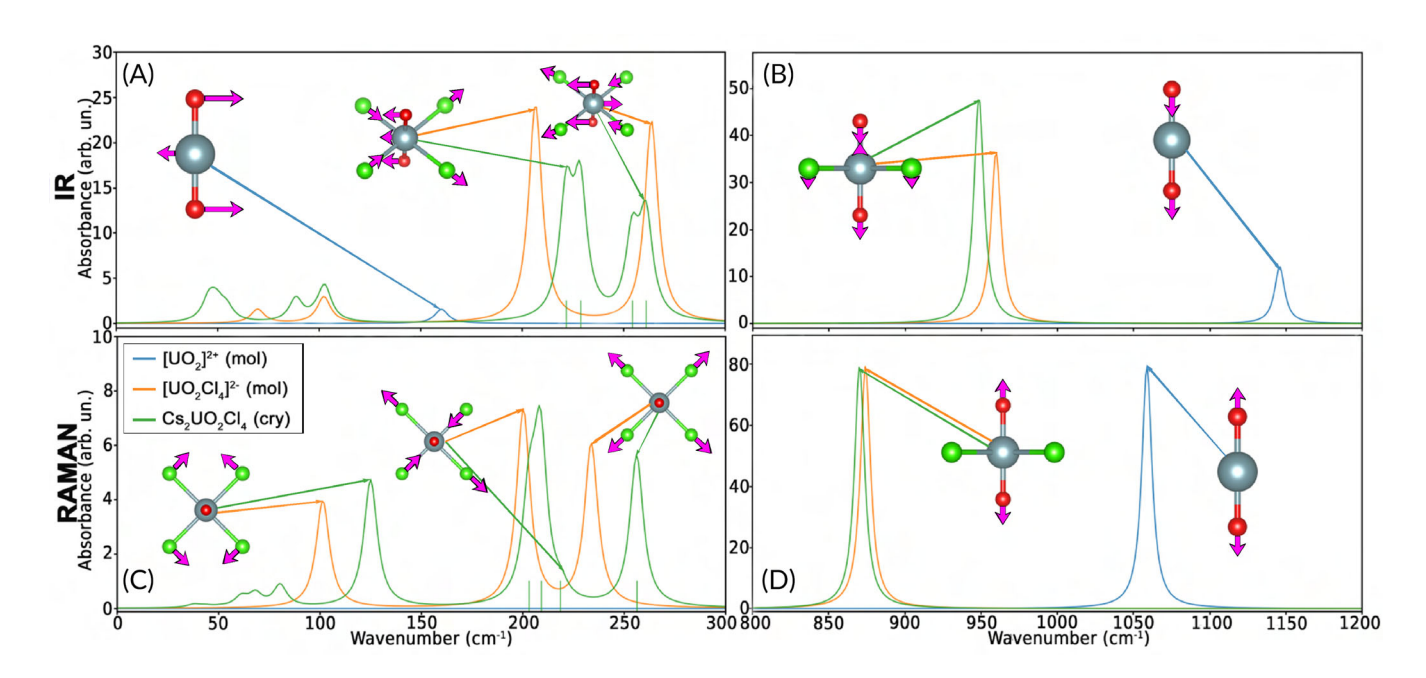
#### 3.1 **Uranyl systems**

Figure 3 displays the IR and Raman spectra of Uranyl based systems in two regions:  $0-300 \text{ cm}^{-1}$  (Figure 3A) and  $800-1200 \text{ cm}^{-1}$  (Figure 3B). Notably, in the IR spectrum for UO<sub>2</sub><sup>2+</sup> (blue line in Figure 3A), two degenerate O-U-O bending modes appear around 160 cm<sup>-1</sup>. An interesting observation arises when CI atoms are introduced into the UO<sub>2</sub>Cl<sub>4</sub><sup>2-</sup> (molecular) and Cs<sub>2</sub>UO<sub>2</sub>Cl<sub>4</sub> (crystal) systems: the O-U-O bending normal mode frequency shifts to the 200-300 cm<sup>-1</sup> range, now encompassing CI-U-CI and O-U-CI angular bending modes as well.

The presence of the four chlorine atoms is found to hinder the bending motion, leading to a blueshift of the peaks in the region comprised between 175 and 300 cm<sup>-1</sup>. Upon further analysis, is observed

**TABLE 1** Bond length (Å identified by *I*) and Bond angles ( $\alpha$  in degrees °) adiabatic force constants (ka) in mdyn/Å for Uranyl (UO<sub>2</sub><sup>2+</sup>), Uranyl Chloride (UO<sub>2</sub>Cl<sub>4</sub><sup>2</sup>) ions and Cs<sub>2</sub>UO<sub>2</sub>Cl<sub>4</sub> periodic system.

Туре		$UO_2^{2+}$	$UO_2Cl_4^{2-}$	Cs <sub>2</sub> UO <sub>2</sub> Cl <sub>4</sub>
U≡O	I	1.70	1.78	1.78
	k <sup>a</sup>	10.734	7.087	6.978
O1-U-O2	α	180.0	180.0	180.0
	k <sup>a</sup>	0.107	0.258	0.251
U-Cl	I	_	2.75	2.71
	k <sup>a</sup>	_	0.798	0.935
O1-U-Cl1	$\alpha$	-	90.0	91.0
	k <sup>a</sup>	-	0.150	0.158
O2-U-Cl1	$\alpha$	-	90.0	89.0
	k <sup>a</sup>	_	0.150	0.174
Cl1-U-Cl2	$\alpha$	-	180.0	180.0
	k <sup>a</sup>	-	0.059	0.068
CI1-U-CI3	$\alpha$	_	90.0	93.5
	k <sup>a</sup>	_	0.062	0.068
CI2-U-CI3	$\alpha$	-	90.0	86.5
	k <sup>a</sup>	-	0.062	0.102



IR and Raman calculated spectra of the  $UO_2^{2+}$  (blue),  $UO_2Cl_4^{2-}$  (orange) and  $Cs_2UO_2Cl_4$  (green) systems: (A) 0–300 cm<sup>-1</sup> region of the IR spectrum alongside the sketches of the O-U-O bending normal modes for the three systems, (B)  $800-1200 \text{ cm}^{-1}$  region of the IR spectrum with the drawings of the  $0 \equiv 0$  asymmetric stretching normal mode. (C)  $0-300 \text{ cm}^{-1}$  of the Raman spectrum side by side with the sketches of U-CI symmetric, asymmetric stretches and CI-U-CI scissoring, (D) 800-1200 cm<sup>-1</sup> of the Raman spectrum next to the  $U\equiv O$ symmetric stretching drawings. The IR spectra peak broadening is computed as a raw superposition of Lorentzian peaks, while the Raman ones are computed using a pseudo-Voigt function. 2 All of the spectra have been produced with the CRYSTALpytool package. 104

that the peak at 206 cm $^{-1}$  of UO $_2$ Cl $_4^{2-}$  ion is related to the mixing of the O–U–O bending and the asymmetric stretching, where the U–Cl bonds stretching is compensated by a slight movement of the Uranium in the same direction of the oxigen atoms. Furthermore, the peak is composed by two degenerate modes corresponding to the two possible directions of the bending motion.

As we transition to the solid-state structure (green line in Figure 3A), the previously observed degeneracy is disrupted, leading to a blueshifted peak. This blueshift can be attributed to alterations in the O–U–Cl and Cl–U–Cl angles induced by the presence of Cs within the system, as indicated by the crystal field details presented in Table 1. A similar observation can be applied to the peak at 263 cm $^{-1}$ , where the two initially degenerate modes represent a combination of O–U–O and Cl–U–Cl bending. Parallel to the earlier observations, the transition to the periodic system also breaks the degeneracy due to changes in the O–U–Cl and Cl–U–Cl angles. However, in this case, the two peaks experience a redshift relative to the UO $_2$ Cl $_4^{2-}$  ion, likely influenced by the slight impediment introduced to the Cl–U–Cl angle due to the presence of Cs within the crystalline structure.

In Figure 3B, the 800–1200 cm $^{-1}$  region of the IR spectrum is depicted for the three systems. Here, three distinct peaks emerge, each corresponding to the asymmetric stretching of the U–O bond within its respective structure. This result is in line with the frequecy reported in a number of experimental and theoretical papers, where the asymmetric stretching of bounded uranyl ions is reported to be in a 830–980 cm $^{-1}$  range. $^{93-96}$  Of notable significance is the conspicuous redshift evident as we transition from the UO $_2$  (blue) ion to the UO $_2$ Cl $_4^{2-}$  and Cs $_2$ UO $_2$ Cl $_4$  systems, represented by the orange and green lines, respectively. This redshift can be attributed to the damping effect induced by the inclusion of four chlorine atoms within the system. Furthermore, the incorporation of Cs atoms within the solid-state system exacerbates the damping of the asymmetric stretching mode, elucidating the subtle red shift observed between the orange and green lines.

Figure 3C illustrates the Raman spectrum in the region comprised between 0 and 300 cm $^{-1}$ , where, once again, the lower wavenumbers region ( < 150 cm $^{-1}$ ) is dominated by the Cs related normal modes and the Cl–U–Cl bendings in scissoring manner ( $\sim \! 100$  cm $^{-1}$ ). At higher wavenumbers ( > 150 cm $^{-1}$ ), instead, the modes are mainly related to the U–Cl symmetric and asymmetric bond stretches. Upon further analysis, we can see that the asymmetric stretching of the U–Cl bond corresponds to the peak at  $\sim \! 197$  cm $^{-1}$  of the UO $_2$ Cl $_4^{2-}$  ion. When we transition to the periodic structure the feature is blue-shifted, probably because the stretching motion both symmetrical and asymmetrical is favored in the crystal by the presence of the counter ion. Following the same analysis, we can attribute the peak at  $\sim \! 233$  cm $^{-1}$  of the orange line to the U–Cl symmetric bond stretching that undergoes an even more significant blue shift in the solid (green).

Figure 3D reports the 800–1200 cm $^{-1}$  region of the Raman spectrum, where, as it happens in same region of the IR spectrum, we can see three peaks, one for each system. These three peaks correspond to the symmetric  $O\equiv U$  bond stretching, reported in literature in a 750–900 cm $^{-1}$  window,  $^{93-96}$  and once more we can notice an evident

red shift when we transition from the uranyl to the uranyl cloride ions. Once again this shift can be related to the dampening induced by the interaction of the four chlorine atoms in the  $\rm UO_2Cl_4^{2-}$  ion that is further aggravated by introducing the Cs atoms in the periodic system.

As we have seen in the spectra analysis, the chemical environment can greatly affect the wavenumber of certain normal modes. Further insight in this phenomenon can be achieved through the analysis of the local force constants provided by the local vibrational theory. If we consider the Uranium Oxigen bonding throughout the three systems in analysis in Table 1the force constant of the bond decreases proportionally to the red shift observed for the U≡O symmetric and asymmetric stretching in the IR and Raman spectra (Figure 3B,D respectively). Such decrease in the force constant would suggest a weakening of the bond due to the introduction of the four chlorine atoms of UO<sub>2</sub>Cl<sub>4</sub><sup>2-</sup> that steal some of the Uranium electron density from the U≡O bond. This is well known in literature as axial equatorial  $\pi$ -competition, <sup>97–99</sup> where a fraction of the electronic density is transferred from the axial bonding region towards both the uranyl oxygen atoms and the equatorial bonding region, effectively weakening the U≡O bond. 94 Such electron density transfer is further reflected in the increase in the bond length probably caused by a weaker electrostatic interaction. At the same time these four chlorine atoms, with their electronic density hinder, the bending of the O-U-O angle leading to a blue shift, as seen in Figure 3A, and a stiffening of the angle reflected in increase of the force constant (Table 1). The introduction of the Cs in the periodic system forces the chlorine atoms off the plane normal to the O-U-O axe leading to a smaller influence of their electronic density with the bending motion as shown by loss of degeneracy and the red shift of the solid with respect to the uranyl chloride ion in Figure 3. All of these effects are also reflected in a decrease of the angle  $k^a$  of the  $Cs_2UO_2Cl_4$ .

In Figure 3A,C we have seen how the peaks related with the symmetric and asymmetric stretching are generally blue shifted when we transition from the uranyl chloride ion to the cesium uranyl cloride. This is probably related with the tilting of the Cl1-U-Cl2 and CI3-U-CI4 axes with respect to the plane normal to the O-U-O plane, that facilitates the stretching motion of the U-Cl bond thanks to a weaker interaction between the electronic clouds of the chlorine atoms. We can see the reflection of these changes in the structure in a shorter U-Cl bond length and a consequent increase in the local force constant of this bond. The slight tilting of Cl1-U-Cl2 and CI3-U-CI4 induced by the Cs atoms in the systems become evident when we take in consideration the O1-U-Cl1 and O2-U-Cl1 angles of 91.0° and 89.0° respectively. These changes, imposed by the Cesium large electronic cloud in the lattice structure, are already present in the structure used as starting point, <sup>100</sup> and they cause a slight increase of the force constants, suggesting a stiffening of both angles, probably induced by the weak interaction of the chlorine atoms with the Cs ones. A further effect induced by the Cesium electron density is the variation of the angles between the equatorial Chlorine atoms in the lattice structure. In the  $UO_2CI_4^{2-}$ , in fact, these atoms are equally spaced with a 90° angle between one another, in the lattice instead we observe a widening of the of Cl1-U-Cl3 angle (Table 1),

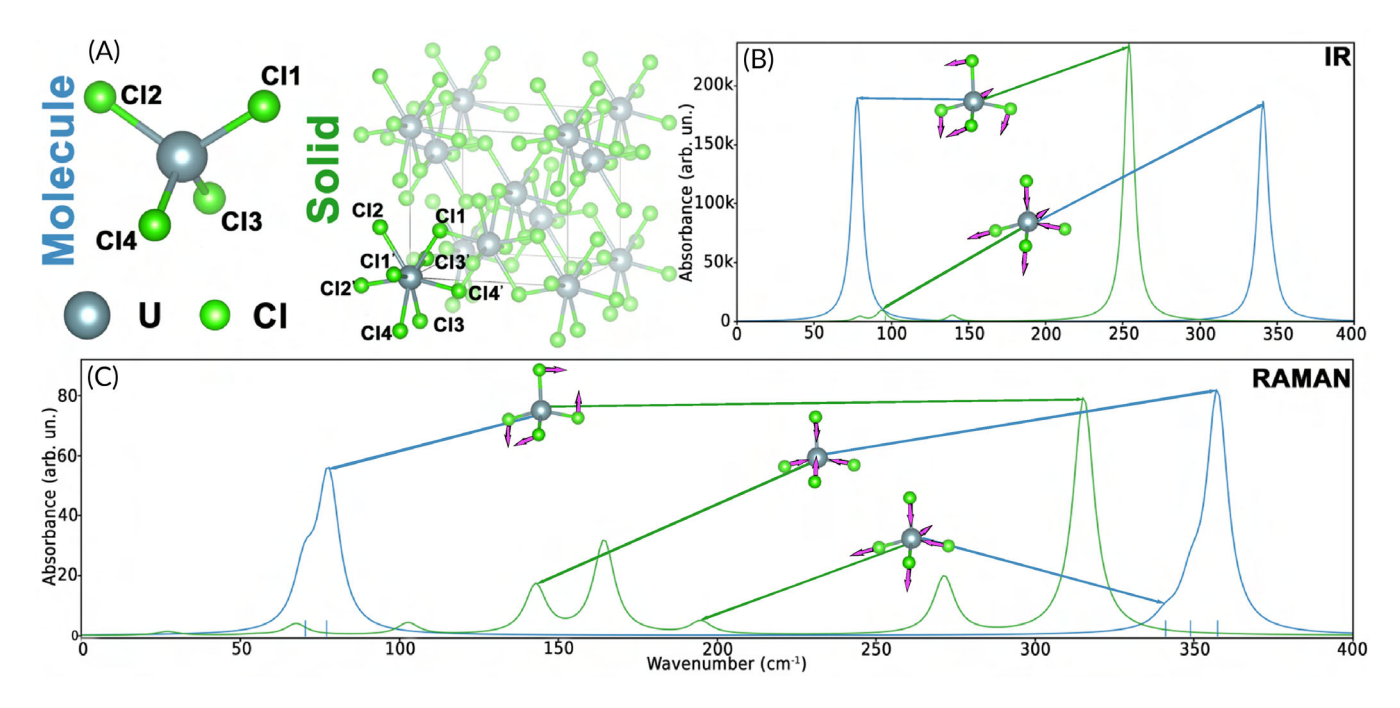


FIGURE 4 Molecular (blue) and Crystalline (green) structure of the Uranium tetrachloride systems alongside IR and Raman calculated spectra of both structure. (A) Molecular (left) and Crystalline (right) structure in its tetragonal lattice (I4<sub>1</sub>/amd) of the UCl<sub>4</sub> systems, where the labeling is kept consistent between molecule and structure for ease of comparison. (B) IR spectra of the two structures reporting the sketches of the asymmetric stretching and bending, where the intensities of the molecular structure have been scaled by a factor of 700 for ease of read purposes. (C) Raman spectra of the two systems alongside the drawing of the scissoring, the symmetric and the asymmetric stretches. The IR spectra peak broadening is computed as a raw superposition of Lorentzian peaks, while the Raman ones are computed using a pseudo-Voigt function. (P2 All of the spectra have been produced with the CRYSTALpytool package.)

where the Cs atom is hosted (Figure 2), and a corresponding narrowing of the Cl3–U–Cl2. Once again these changes imposed by the lattice structure are reflected in the blue shift of the scissoring motion of the chlorine atoms and the relative force constants: the Cl1–U–Cl3 angle seems to be slightly more rigid due to lattice constrains, the narrower Cl3–U–Cl2 angle force constant, instead, has a larger increase between the molecular ion and the periodic structure. This ladder effect probably can be explained with two opposite Cs electronic cloud pushing against the Chlorine atoms and making the angle stiffer.

# 3.2 | Uranium chloride systems

The second set of systems we examined includes uranium tetrachloride in both its molecular and periodic forms, with their structures shown in Figure 4A. For both of these systems, calculations were conducted on fully relaxed structures, with the only constraint imposed being the symmetry of  $I4_1/amd$  tetragonal phase in the solid.

To gain a deeper understanding into the force constants, we initiate our analysis by examining the IR and Raman spectra of the structure, which are presented in Figure 4B,C. The IR spectrum (Figure 4B) shows two prominent peaks for the molecular structure in blue, one at 340 cm<sup>-1</sup> and the other at 78 cm<sup>-1</sup>. The first can be easily assigned to the asymmetric stretching of the system, where two bonds U–CI are elongated, while the other two become shorter. This

is in line with a number of experimental and theoretical studies, where this is reported in a window comprised between 320 and 350 cm<sup>-1</sup>. <sup>101-103</sup> When we transition to the periodic system (green) this peak undergoes a strong redshift, where it is shifted to 96 cm<sup>-1</sup> due to the strongly hindered stretching of the bonds induced by the crystalline structure, as each chlorine is shared between two Uranium atoms. The opposite trend can be observed for the peak at 78 cm<sup>-1</sup> (blue) which corresponds to the bending of the molecule and it undergoes a strong blueshift when we move to the solid state structure at 255 cm<sup>-1</sup>. As for the shift of the asymmetric stretching, also this blueshift can be explained with the constrains imposed by the periodic structure that hinders the bending motion allowing for a shorter travel at a higher frequency with respect to the molecular structure.

In Figure 4C, the Raman spectra of the molecule are displayed, showcasing two primary peaks (blue) for the molecular structure. The first peak resides within the 340–360 cm<sup>-1</sup> range, corresponding to both the symmetric (shoulders at 341 cm<sup>-1</sup>) and asymmetric (peak at 357 cm<sup>-1</sup>) stretching modes. <sup>101–103</sup> The second peak, discernible in the bending vibrations, emerges within the 50–100 cm<sup>-1</sup> region. The analysis of the Raman spectra of the crystalline structure (green), once more, reveals a strong redshift of the stretches and a comparable blueshift of the bendings, both due to the restrained motion allowed by the lattice structure. The symmetric stretching that, in the molecule, falls at 357 cm<sup>-1</sup>, in the solid (green), gets mixed up with the

**TABLE 2** Bond length (Å identified by I) and Bond angles ( $\alpha$  in degrees °) adiabatic force constants ( $k^a$ ) in mdyn/Å for the Uranium Chloride system both in its molecular and crystalline form.

Туре		Mol.	Cry (1st)	Cry (2nd)
U-CI	1	2.49	2.64	2.91
	k <sup>a</sup>	2.134	0.554	0.130
Cl2-U-Cl1	α	114.3	92.4	66.3
	k <sup>a</sup>	0.053	0.051	0.265
CI2-U-CI4	α	107.1	156.4	134.5
	$k^a$	0.048	0.101	0.091

bending, as imposed by the crystalline, and it is shifted to lower energy (143 cm<sup>-1</sup>).

It is noted that the transition to the solid-state introduces a second coordination sphere, with four additional chlorine atoms interacting with the original uranium at a distance of 2.91 Å. These additional atoms, forming the second neighbor sphere, simultaneously serve as the first neighbors of adjacent uranium atoms, resulting in the formation of U-Clx-U' angles. This new conformation prevents the pure stretching modes as each Chlorine is shared by two Uranium atoms, the stretching of one of the two coordination spheres will correspond to the bending in the other one. The bendings, on the other hand, can be pure, also for the crystalline structure since the motion is not directed along the bonds. The solid phase, though, will hinder a large motion, allowing only a shorter travel distance at a higher frequency, thus causing a strong blue shift like the one observed for the scissoring of the system that we can find at 77 cm<sup>-1</sup>, in the molecule, and at 315 cm<sup>-1</sup>, in the crystal.

As noted, similar to the observations in the Uranyl systems, the crystalline structure also introduces variations to the structural parameters of the UCl<sub>4</sub> molecular unit. In its periodic structure, the UCl<sub>4</sub> undergoes a change in the coordination sphere around the Uranium atoms. Specifically, the Uranium atoms are now bonded to eight Chlorine atoms, forming two distinct coordination spheres, each comprising four atoms. A similar change in coordination is also evident for the Chlorine atoms, which now form bonds with two Uranium atoms, each exhibiting two distinct bond lengths. These changes in coordination are also reflected in the force constants, as presented in Table 2. The two coordination spheres around Uranium are discernible through the two different bond lengths: 2.64 and 2.91 Å, respectively. The elongation of the bond length correlates with a significant reduction in the respective local force constants of the U-Cl bond. This force constant decreases from 2.134 mdyn/Å in the molecule to 0.554 and 0.130 mdyn/Å for the first and second coordination spheres, respectively. This decrease is driven by the pronounced redshift observed in the stretching frequencies within the spectra (Figure 4).

When we consider the angles inside the tetrahedral unit of the UCl<sub>4</sub>, we can see the second change imposed by the transition to the solid-state of the system. In fact, the Cl2-U-Cl1 angle becomes narrower in the crystal for both sphere of coordination. Such

tightening of the angle is reflected in an increase of the  $k^a$  corresponding to a large blue shift of the bending in the spectra. The CI2-U-CI4 angle, instead, is widened in the periodic structure, with a corresponding increase in the force constant again related with the blueshift of the bending related peaks. Moreover, the increase of the local force constants related to the angle is probably induced by the presence of a chemical surrounding in the periodic structure, that strongly hinders the motion of the structure with respect to the molecular one.

# 4 | CONCLUSIONS

This paper introduced the implementation of the LModeA package for analyzing 2D/3D periodic systems and its integration with the CRYSTAL package. The investigation dealt with uranium-based systems, and considered two distinct case studies. The first case study explored the uranyl ion ( $UO_2^{2+}$ ) and its transformation towards the solid state, culminating in the  $Cs_2UO_2Cl_4$  form through the intermediate uranyl chloride ion ( $UO_2Cl_4^{2-}$ ). In the second case study, the focus shifted to the uranium chloride ( $UCl_4$ ) system in both molecular and periodic forms. The analysis focused on the infrared (IR) and Raman harmonic spectra, examining how they are affected by the transition to the solid state.

The newly developed interface between the LModeA code and the CRYSTAL package for DFT ab-initio simulation, allowed a smooth workflow for the study of solid state systems, providing a single tool for both molecules and solids. Moreover, its application showcased the great potential of LVM analysis for the study of complex materials, providing valuable insights to be used for their fine-tuning and the design of new materials. The data obtained for our test systems comparing both molecular and periodic forms, reveal the interesting finding that the change of the structural unit imposed by the crystal field results in a general red-shift of the normal vibrational bond stretching modes and a blue-shift of the bending modes. These shifts observed both in the IR and Raman spectra are reflected by the local mode force constants  $k^a$  of the different systems. Thus we showed how  $k^a$ is effectively able to reproduce packing effects and how it can be effectively used as a bond strength indicator also for periodic systems, independently from the nature of the crystal.

### **ACKNOWLEDGMENTS**

We thank SMU's Center for Research Computing for providing generous computational resources. Elfi Kraka thanks the National Science Foundation for support; Grant CHE 2102461. Filippo Bodo and Alessandro Erba acknowledge that this research has received funding from the Project CH4.0 under the MUR program "Dipartimenti di Eccellenza 2023-2027" (CUP: D13C22003520001). Filippo Bodo is grateful to Dr Jefferson Maul for fruitful scientific discussions. Renaldo T. Moura Jr. thanks the Brazilian Public Call n. 03 "Produtividade em Pesquisa" PROPESQ/PRPG/UFPB project number PVN13305-2020.

### **DATA AVAILABILITY STATEMENT**

The data that support the findings of this study are available from the corresponding author upon reasonable request.

### ORCID

Filippo Bodo https://orcid.org/0000-0002-8422-6618

Alessandro Erba https://orcid.org/0000-0002-2986-4254

Elfi Kraka https://orcid.org/0000-0002-9658-5626

Renaldo T. Moura Jr. https://orcid.org/0000-0002-8151-1640

### REFERENCES

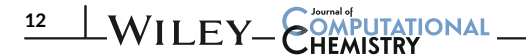
- [1] L. Pauling, J. Chem. Educ. 1992, 69, 519.
- [2] K. Ruedenberg, Rev. Mod. Phys. 1962, 34, 326.
- [3] G. Frenking, S. Shaik, The chemical bond: fundamental aspects of chemical bonding, John Wiley & Sons, Hoboken, New Jersey 2014.
- [4] F. Weinhold, Encycloped Comput Chem 2002, 3, 1792.
- [5] F. Weigend, R. Ahlrichs, Phys. Chem. Chem. Phys. 2005, 7, 3297.
- [6] F. Weinhold, C. Landis, E. Glendening, Int. Rev. Phys. Chem. 2016, 35, 399.
- [7] E. D. Glendening, C. R. Landis, F. Weinhold, Wiley Interdiscip. Rev: Comput. Mol. Sci. 2012, 2, 1.
- [8] E. D. Glendening, C. R. Landis, F. Weinhold, J. Comput. Chem. 2019, 40, 2234.
- [9] R. F. Bader, Acc. Chem. Res. 1985, 18, 9.
- [10] R. Bader, Atoms in molecules, Oxford Press, Oxford, UK 1990.
- [11] R. F. Bader, Chem. Rev. 1991, 91, 893.
- [12] R. F. Bader, J Phys Chem A 1998, 102, 7314.
- [13] R. F. Bader, C. F. Matta, J Phys Chem A 2004, 108, 8385.
- [14] F. Cortés-Guzmán, J. I. Rodríguez, J. S. Anderson, Advances in quantum chemical topology beyond QTAIM, Elsevier, Amsterdam, NL 2023 p. 1
- [15] Y.-R. Luo, Handbook of bond dissociation energies in organic compounds, CRC Press, Boca Raton, Florida 2002.
- [16] S. J. Blanksby, G. B. Ellison, Acc. Chem. Res. 2003, 36, 255.
- [17] M. D. Morse, Acc. Chem. Res. 2018, 52, 119.
- [18] D. Cremer, E. Kraka, Curr. Org. Chem. 2010, 14, 1524.
- [19] D. Cremer, E. Kraka, Dalton Trans. 2017, 46, 8323.
- [20] Z. Konkoli, D. Cremer, Int. J. Quantum Chem. 1998a, 67, 1.
- [21] E. Kraka, W. Zou, Y. Tao, WIREs Comput. Mol. Sci. 2020, 10, 1480.
- [22] E. Kraka, M. Quintano, H. W. L. Force, J. J. Antonio, M. Freindorf, J. Phys. Chem. A 2022, 126, 8781.
- [23] R. T. Moura Jr., M. Quintano, J. J. Antonio, M. Freindorf, E. Kraka, J. Phys. Chem. A 2022, 126, 9313.
- [24] D. Cremer, A. Wu, J. A. Larsson, E. Kraka, J. Mol. Model. 2000, 6, 396.
- [25] E. Kraka, D. Cremer, Int. J. Quantum Chem. 2019, 119, e25849.
- [26] Z. Konkoli, J. A. Larsson, D. Cremer, Int. J. Quantum Chem. 1998a, 67, 11.
- [27] Z. Konkoli, D. Cremer, Int. J. Quantum Chem. 1998b, 67, 29.
- [28] Z. Konkoli, J. A. Larsson, D. Cremer, Int. J. Quantum Chem. 1998b, 67, 41
- [29] Y. Tao, C. Tian, N. Verma, W. Zou, C. Wang, D. Cremer, E. Kraka, J. Chem. Theory Comput. 2018, 14, 2558.
- [30] M. Quintano, E. Kraka, Chem. Phys. Lett. 2022, 803, 139746.
- [31] N. Verma, Y. Tao, W. Zou, X. Chen, X. Chen, M. Freindorf, E. Kraka, Sensors 2020, 20, 2358.
- [32] M. Quintano, A. A. A. Delgado, R. T. Moura Jr., M. Freindorf, E. Kraka, Electron. Struct. 2022, 4, 044005.
- [33] M. Freindorf, A. A. A. Delgado, E. Kraka, J. Comput. Chem. 2022, 43, 1725.
- [34] R. T. Moura Jr., M. Quintano, C. V. Santos-Jr, V. A. Albuquerque, E. C. Aguiar, E. Kraka, A. N. Carneiro Neto, Optic Mater: X 2022, 16, 100216.
- [35] A. Madushanka, R. T. Moura Jr., N. Verma, E. Kraka, Int. J. Mol. Sci. 2023, 24, 6311.
- [36] A. Cossard, J. K. Desmarais, S. Casassa, C. Gatti, A. Erba, J Phys Chem Lett 2021a, 12, 1862.

- [37] A. Cossard, S. Casassa, C. Gatti, J. K. Desmarais, A. Erba, Molecules 2021b, 26, 4227.
- [38] A. Otero-de-la Roza, V. Luaña, J. Comput. Chem. 2011, 32, 291.
- [39] A. Otero-de-la Roza, E. R. Johnson, V. Luaña, Comput. Phys. Commun. 2014, 185, 1007.
- [40] N. Marzari, D. Vanderbilt, Phys. Rev. B 1997, 56, 12847.
- [41] P. L. Silvestrelli, N. Marzari, D. Vanderbilt, M. Parrinello, Solid State Commun. 1998, 107, 7.
- [42] I. Souza, N. Marzari, D. Vanderbilt, Phys. Rev. B 2001, 65, 035109.
- [43] N. Marzari, A. A. Mostofi, J. R. Yates, I. Souza, D. Vanderbilt, Rev. Mod. Phys. 2012, 84, 1419.
- [44] R. Dronskowski, P. E. Blöchl, J. Phys. Chem. 1993, 97, 8617.
- [45] T. Hughbanks, R. Hoffmann, J. Am. Chem. Soc. 1983, 105, 3528.
- [46] M. T. Ruggiero, A. Erba, R. Orlando, T. M. Korter, Phys. Chem. Chem. Phys. 2015, 17, 31023.
- [47] M. T. Ruggiero, J. Sibik, A. Erba, J. A. Zeitler, T. M. Korter, Phys. Chem. Chem. Phys. 2017, 19, 28647.
- [48] R. Y. Rohling, I. C. Tranca, E. J. Hensen, E. A. Pidko, J Phys Chem C 2019, 123, 2843.
- [49] J. Waser, L. Pauling, J Chem Phys 1950, 18, 747.
- [50] Y. Tao, W. Zou, S. Nanayakkara, E. Kraka, J. Chem. Theory Comput. 2022, 18, 1821.
- [51] N. Tadaaki, K. Kazuo, I. Yoshitaka, O. Chuhei, S. Otani, Surf. Sci. 1993, 290, 436.
- [52] H. Gupta, M. K. Singh, L. Tiwari, J. Solid State Chem. 2000, 153, 317.
- [53] T. Aizawa, W. Hayami, S. Otani, Phys. Rev. B 2001, 65, 024303.
- [54] S. M. Aarons, N. Dauphas, M. Blanchard, H. Zeng, N. X. Nie, A. C. Johnson, N. D. Greber, T. Hopp, ACS Earth Space Chem 2021, 5, 2466.
- [55] C. Lee, X. Gonze, Phys. Rev. Lett. 1994, 72, 1686.
- [56] A. Tapia, C. Cab, A. Hernández-Pérez, C. Villanueva, F. Peñuñuri, F. Avilés, Phys E: Low-Dimen Syst Nanostruct 2017, 89, 183.
- [57] A. Shyichuk, R. T. Moura Jr., A. N. C. Neto, M. Runowski, M. S. Zarad, A. Szczeszak, S. Lis, O. L. Malta, J Phys Chem C 2016, 120, 28497.
- [58] Y. Tao, W. Zou, D. Sethio, N. Verma, Y. Qiu, C. Tian, D. Cremer, E. Kraka, J. Chem. Theory Comput. 2019, 15, 1761.
- [59] W. Zou, R. Moura Jr., M. Quintano, F. Bodo, Y. Tao, M. Freindorf, M. Z. Makoś, N. Verma, D. Cremer, E. Kraka, LModeA2023, Computational and Theoretical Chemistry Group (CATCO), Southern Methodist University, Dallas, TX, USA 2023a.
- [60] A. Erba, J. K. Desmarais, S. Casassa, B. Civalleri, L. Donà, I. J. Bush, B. Searle, L. Maschio, L. Edith-Daga, A. Cossard, et al., J. Chem. Theory Comput. 2023, 19, 6891–6932.
- [61] P. Söderlind, G. Kotliar, K. Haule, P. M. Oppeneer, D. Guillaumont, MRS Bull. 2010, 35, 883.
- [62] T. Vitova, I. Pidchenko, D. Fellhauer, P. S. Bagus, Y. Joly, T. Pruessmann, S. Bahl, E. Gonzalez-Robles, J. Rothe, M. Altmaier, et al., Nat. Commun. 2017, 8, 16053.
- [63] M. L. Neidig, D. L. Clark, R. L. Martin, Coord. Chem. Rev. 2013, 257, 394.
- [64] I. Crossland, Nuclear fuel cycle science and engineering, Elsevier, Amsterdam, NL 2012.
- [65] Y. Hu, Z. Shen, B. Li, X. Tan, B. Han, Z. Ji, J. Wang, G. Zhao, X. Wang, J. Hazard. Mater. 2022, 426, 127838.
- [66] E. B. Wilson, J. Chem. Phys. 1941, 9, 76.
- [67] E. B. Wilson, J. C. Decius, P. C. Cross, Molecular vibrations: the theory of infrared and Raman vibrational spectra, McGraw-Hill, New York 1955.
- [68] W. Zou, R. Kalescky, E. Kraka, D. Cremer, J. Chem. Phys. 2012a, 137, 084114.
- [69] Y. Tao, Y. Qiu, W. Zou, S. Nanayakkara, S. Yannacone, E. Kraka, Molecules 2020, 25, 1589.
- [70] E. B. Wilson, J. C. Decius, P. C. Cross, Molecular vibrations: the theory of infrared and Raman vibrational spectra, Courier Corporation, Garden City, New York 1980.

- [71] E. Balan, J. Kloprogge, Developments in Clay Science, Vol. 8, Elsevier, Amsterdam, NL 2017, p. 6.
- [72] L. A. Woodward, Introduction to the theory of molecular vibrations and vibrational spectroscopy, Oxford University Press, Oxford 1972.
- [73] S. Califano, Vibrational states, Wiley, New York 1976.
- [74] R. J. Meier, Vib. Spectros. 2007, 43, 26.
- [75] W. Zou, D. Izotov, D. Cremer, J. Phys. Chem. A 2011, 115, 8731.
- [76] W. Zou, M. Filatov, D. Cremer, Int. J. Quantum Chem. 2012b, 112, 3277.
- [77] W. Zou, D. Cremer, Aust. J. Chem. 2014, 67, 435.
- [78] D. Cremer, J. A. Pople, J. Am. Chem. Soc. 1975, 97, 1354.
- [79] W. Zou, M. Freindorf, V. Oliveira, Y. Tao, E. Kraka, Can. J. Chem. 2023b. https://doi.org/10.1139/cjc-2022-0254
- [80] J. J. Antonio, E. Kraka, Biochemistry 2023, 62, 2325. https://doi.org/ 10.1021/acs.biochem.3c00192
- [81] B. M. T. C. Peluzo, M. Z. Makoś, R. T. Moura Jr., M. Freindorf, E. Kraka, *Inorg. Chem.* 2023, 62, 12510. https://doi.org/10.1021/acs.inorgchem.3c01761
- [82] P. Groner, Normal coordinate analysis, John Wiley, New York 2006.
- [83] J. D. Kelley, J. J. Leventhal, Problems in classical and quantum mechanics, Springer, Berlin, Germany 2017, p. 95.
- [84] W. Zou, D. Cremer, Chem. Eur. J. 2016, 22, 4087.
- [85] M. I. Aroyo, International tables for crystallography, Wiley Online Library, Hoboken, New Jersey 2013.
- [86] A. D. Becke, J. Chem. Phys. 1993, 98, 5648.
- [87] M. Dolg, Theor Comput Chem 2002, 11, 793.
- [88] M. Dolg, X. Cao, J Phys Chem A 2009, 113, 12573.
- [89] B. Sadhu, M. Dolg, M. S. Kulkarni, J. Comput. Chem. 2020, 41, 1427.
- [90] R. Ponec, L. Bučinský, C. Gatti, J. Chem. Theory Comput. 2010, 6, 3113.

- [91] W. R. Wadt, P. J. Hay, J Chem Phys 1985, 82, 284.
- [92] R. Dovesi, V. Saunders, C. Roetti, R. Orlando, C. Zicovich-Wilson, F. Pascale, B. Civalleri, K. Doll, N. Harrison, I. Bush, et al. (2023).
- [93] L. Maya, G. Begun, J. Inorg. Nucl. Chem. 1981, 43, 2827.
- [94] P. Di Pietro, A. Kerridge, Inorg. Chem. 2016, 55, 573.
- [95] G. Lu, A. J. Haes, T. Z. Forbes, Coord. Chem. Rev. 2018, 374, 314.
- [96] G. Lu, T. Z. Forbes, A. J. Haes, Anal. Chem. 2016, 88, 773.
- [97] G. Schreckenbach, P. J. Hay, R. L. Martin, Inorg. Chem. 1998, 37, 4442
- [98] S. Fortier, T. W. Hayton, Coord. Chem. Rev. 2010, 254, 197.
- [99] K. I. Ingram, L. J. L. Häller, N. Kaltsoyannis, Dalton Trans. 2006, 2403.
- [100] V. V. Zhurov, E. A. Zhurova, A. A. Pinkerton, *Inorg. Chem.* 2011, 50, 6330.
- [101] S. A. Arthers, I. R. Beattie, J. Chem. Soc., Dalton Trans. 1984, 819.
- [102] M. Shundalau, P. Chybirai, A. Komyak, A. Zazhogin, D. Umreiko, J. Appl. Spectrosc. 2012, 79, 165.
- [103] H. VidaráVolden, J. Rudy, J. Chem. Soc., Dalton Trans. 1995, 185.
- [104] B. Camino, H. Zhou, E. Ascrizzi, A. Boccuni, F. Bodo, A. Cossard, D. Mitoli, A. M. Ferrari, A. Erba, N. M. Harrison, Comput. Phys. Commun. 2023, 292, 108853.

How to cite this article: F. Bodo, A. Erba, E. Kraka, R. T. Moura Jr., J. Comput. Chem. **2024**, 1. <a href="https://doi.org/10.1002/jcc.27311">https://doi.org/10.1002/jcc.27311</a>



### **APPENDIX**

The main development in the LModeA code that we presented in this work is the new interface with the CRYSTAL package for DFT ab initio

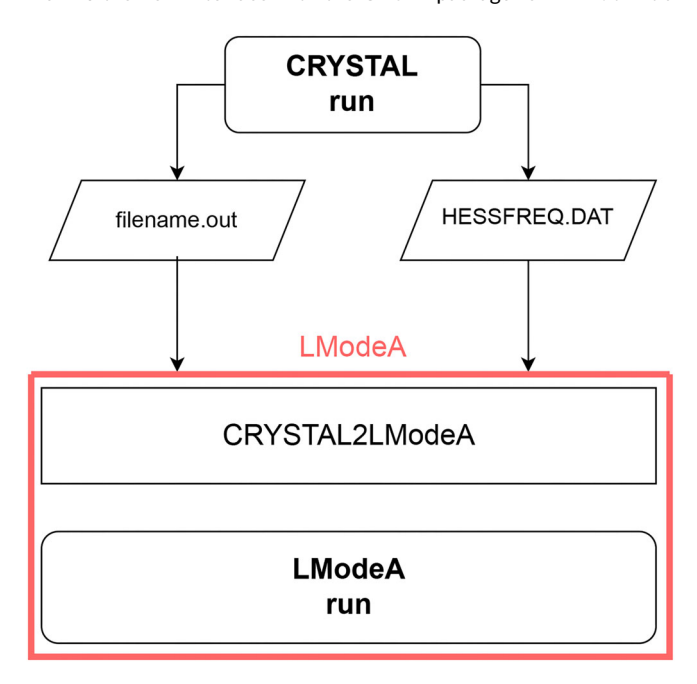


**FIGURE A1** Flowchart of the CRYSTAL2LModeA interface showing the workflow starting from the CRYSTAL frequency calculation to the LModeA calculation.

simulations on solids. Thus we want to provide here an idea of how the code works and what are the necessary steps that a user should follow

The aim of the new CRYSTAL2LModeA interface is to add the compatibility with the CRYSTAL package without disrupting the already well known input system of the LModeA code, allowing for a smoother workflow as shown in Figure A1. This is achieved through a function in the new LModeA python wrapper that was included in its latest version (v3.0.0). Thus, the user can run the LModeA code starting from a CRYSTAL frequency calculation setting the qcprog keyword in the \$contrl section of the input equal to ~CRYSTAL~. Furthermore, in the \$qcdata section the user will have to define the files containing the geometry and the Hessian of the system of interest as follows: GEOM=~filename.out~ and HESS=~HESSFREQ.DAT~.

Once the LModeA calculation is launched the code will extract from the filename.out the atoms number and nuclear charges, their coordinates in Å in the primitive cell or the molecule object of the calculation and their masses used in calculation, alongside the kind of calculation (Figure A2 step 1). Then, the CRYSTAL2LModeA script will extract the Hessian of the system from the HESSFREQ.DAT unit. If the calculation is periodic, step 2 Figure A2, the LModeA code will proceed to drop the translation mode of the system and perform the Local Mode Analysis. Otherwise, in case of a molecular calculation, the code will perform the analysis dropping both translations and rotations of the system.

### Algorithm 1 CRYSTAL2LModeA interface

- 1. Reads data from the frequency calculation filename.out and HESSFREQ.DAT unit.
  - From the filename.out:
    - Number of atoms
    - Atomic masses
    - Atomic charges
    - Atomic coordinates of the primitive cell (or molecule) in Å
    - Atomic masses used in the calculation
    - Type of calculation (molecular or periodic)
  - From the HESSFREQ.DAT unit:
    - Hessian of the system.
- 2. if periodic == True then
  - $\bullet\,$  Drops the three modes related to the translations
  - Retains the three rotations
  - Performs Local Mode Analysis

end

else

- Drops both rotation and translations
- Performs Local Mode Analysis

end

FIGURE A2 Illustrative scheme of the interface between the LModeA code and CRYSTAL package for solid sate DFT *ab initio* simulation: (step 1) Extraction of the data required for the LModeA calculation from the CRYSTAL frequency calculation filename.out and the HESSFREQ.DAT unit. (step 2) How the Local Mode Analysis is performed for periodic and molecular case respectively.

It is important to notice that step **2** of Figure A2 is available for all *ab initio* solid state packages through the ALMODE data file, where the user needs to specify the number of atoms in the system, their

masses, their nuclear charges, the atomic coordinates of the primitive cell or molecule in  $\mathring{A}$ , the Hessian of the system and, in case of solids, the periodic nature of the system.